

On the rigidity of back-to-back top quark pairs in e^+e^- annihilation

S. Groote, J.G. Körner and J.A. Leyva¹

Institut für Physik, Johannes-Gutenberg-Universität,
Staudinger Weg 7, D-55099 Mainz, Germany

Abstract

We consider the effect of gluon radiation on the energy of top/antitop quarks and on the anticollinearity of top-antitop quark pairs produced in e^+e^- annihilation. Our results are presented in terms of the E_q -dependence of the $t\bar{t}g$ cross section and the dependence on the cosine of the opening angle θ_{12} between top and antitop for a center of mass energy of $\sqrt{q^2} = 500 \text{ GeV}$. We then go on to determine mean values for the top quark's energy as well as its longitudinal and transverse projections, and for the deviation of $\sin \theta_{12}$ and $\cos \theta_{12}$ from the anticollinearity limits $\sin \theta_{12} = 0$ and $\cos \theta_{12} = -1$. For a center of mass energy of 500 GeV we obtain $\langle E_q \rangle = 248.22 \text{ GeV}$, $\langle E_L \rangle = 247.24 \text{ GeV}$ and $\langle E_T \rangle = 4.70 \text{ GeV}$. Thus, at this energy gluon radiation causes a total average energy loss of 0.71% of the top quark's energy. The average energy loss in the longitudinal direction is 1.06% and the average energy gain in the transverse direction is 1.88%. These percentage figures go up to 3.77%, 5.19% and 6.06%, respectively, at 1000 GeV . For the mean of the acollinearity angle $\bar{\theta}_{12} = 180^\circ - \theta_{12}$ we obtain $\langle \bar{\theta}_{12} \rangle = 1.25^\circ$ at 500 GeV , the value of which goes up to 4.62° at 1000 GeV . From an analysis of the transverse momentum of the top we find that the mean transverse momentum of the top stays close to the mean total momentum of the gluon in the energy range from threshold to 1000 GeV showing that the gluon momentum has a large mean transverse component in this energy range.

¹On leave of absence from CIF, Bogotá, Colombia

1 Introduction

Top quark pairs produced in e^+e^- annihilation provide a very clean and kinematically well-defined source of top quarks. To leading order in the QCD coupling constant α_s the energy of the top quark is exactly given by one-half of the center of mass energy. The top and antitop quarks decay so fast that there is no visible primary track. Even if the energy of the top quark is constrained by the beam energy one has to rely on kinematical reconstruction from an analysis of the decay products in order to pin down the momentum direction of the primary top quark pairs. Since to lowest order of QCD the top and antitop are produced exactly back-to-back, the lowest order anticollinearity provides for a further important kinematical constraint on the production kinematics.

An exact knowledge of the momentum configuration of the primary produced top quark pairs is important for measurements of the spin observables of the top quark. If the top quark's momentum and momentum direction is known, one can boost to the rest frame of the top quark and do the spin analysis in the top quark rest system which is the optimal frame from the point of view of a spin analysis. As concerns spin-spin correlation effects, the anticollinearity of the produced top quark pairs is also important for optimizing spin-spin correlation measurements [1].

Previously it has been emphasized that the bremsstrahlung of gluons off the top quark pairs can have important effects on various characteristics of the $t\bar{t}$ final state. For example, the mass determination of the top quark and the energy spectrum of secondary leptons will be affected by the presence of gluon bremsstrahlung [2, 3, 4]. In order to quantify the effect of gluon bremsstrahlung, the authors of [5] have calculated the gluon energy spectrum in $e^+e^- \rightarrow t\bar{t}g$ as well as the mean energy of the gluon $\langle E_g \rangle$. Having in mind the above-mentioned spin analysis we continue in the study of gluon emission effects in $e^+e^- \rightarrow t\bar{t}g$ and determine how the energy of the top (or antitop) quark is affected by gluon emission and how the anticollinearity of the top-antitop configuration is distorted by gluon emission.

Our paper is structured as follows. In Sec. 2 we study the top energy spectrum and compare it to the bottom energy spectrum. From this we determine the mean deviation of the top and bottom energy E_q from their lowest order value $\frac{1}{2}\sqrt{q^2}$. A simple analysis shows that the mean quark energy $\langle E_q \rangle$ is related to the mean gluon energy $\langle E_g \rangle$ calculated in [5]. Although this result is quite plausible at first sight it is nevertheless surprising since the calculation of the gluon's mean energy $\langle E_g \rangle$ involves tree graph contributions only whereas one needs to bring in loop contributions for the determination of the quark's mean energy $\langle E_q \rangle$. In Sec. 3 we check on the rigidity of the back-to-back top quark pair configuration against gluon radiation by looking at opening angle distributions and their mean values. We determine the differential $\cos \theta_{12}$ -distribution where θ_{12} is the opening angle of the top quark pair and compare to the corresponding distribution in the bottom quark case. We then go on to calculate the mean deviations of $\cos \theta_{12}$ and $\sin \theta_{12}$ from the anticollinearity limits $\cos \theta_{12} = -1$ and $\sin \theta_{12} = 0$. In Sec. 4 we study mean values of the longitudinal energy E_L and the transverse energy E_T of the top quark. The leading contributions to these measures are given by the mean energy $\langle E_q \rangle$ calculated in Sec. 2 and

by the mean opening angle measures $\langle 1 + \cos \theta_{12} \rangle$ and $\langle \sin \theta_{12} \rangle$ calculated in Sec. 4. We also numerically evaluate the mean transverse momentum $\langle p_T \rangle$ of the top quark relative to the antitop direction and the mean of the opening angle itself. Sec. 5 contains our summary and conclusions. In Appendix A we list explicit formulas for the full $O(\alpha_s)$ heavy quark production cross section which enter in the evaluation of the mean values as denominator functions. In Appendix B we list a number of basic rate functions which appear in our analytical results. In Appendix C we present analytical results on first moment integrals that are needed for the evaluation of the mean values of $\langle E_q \rangle$ and $\langle 1 + \cos \theta_{12} \rangle$ for scalar and pseudoscalar current-induced top pair production.

2 Quark energy spectrum and $\langle E_q \rangle$

To begin with we express the differential heavy quark production cross section in $e^+e^- \rightarrow q(p_1)\bar{q}(p_2)g(p_3)$ with $q = p_1 + p_2 + p_3$ in terms of the relevant components of the hadron tensor $H^i = (-g^{\mu\nu} + q^\mu q^\nu / q^2)H_{\mu\nu}^i$

$$\frac{d\sigma}{dy dz} = \frac{\alpha^2}{48\pi q^2} \left(g_{11} H^1(y, z) + g_{12} H^2(y, z) \right) \quad (1)$$

where $y = 1 - 2p_1q/q^2$ and $z = 1 - 2p_2q/q^2$ are fractional energy loss variables for the heavy quark and antiquark. We shall also use the abbreviation $\xi = 4m_q^2/q^2$. Another useful variable is the Born term velocity of the quark given by $v = \sqrt{1 - \xi}$. We closely follow the notation employed in [6]. Thus the superfix $i = 1, 2$ stands for the two current combinations $H^1 = \frac{1}{2}(H^{VV} + H^{AA})$ and $H^2 = \frac{1}{2}(H^{VV} - H^{AA})$. In Eq. (1) we have already averaged over the relative beam-event orientation. In the terminology of [6] the full hadron tensor components would thus carry the additional index ($U + L$) relevant to the total rate (U : unpolarized transverse, L : longitudinal). However, since we are only concerned with the total rate in this paper we have consistently dropped this index. The parameters g_{11} and g_{12} specify the electro-weak model dependence and are given by

$$\begin{aligned} g_{11} &= Q_f^2 - 2Q_f v_e v_f \text{Re } \chi_Z + (v_e^2 + a_e^2)(v_f^2 + a_f^2) |\chi_Z|^2, \\ g_{12} &= Q_f^2 - 2Q_f v_e v_f \text{Re } \chi_Z + (v_e^2 + a_e^2)(v_f^2 - a_f^2) |\chi_Z|^2, \end{aligned} \quad (2)$$

where, in the Standard Model, $\chi_Z(q^2) = gM_Z^2 q^2 (q^2 - M_Z^2 + iM_Z \Gamma_Z)^{-1}$, with M_Z and Γ_Z the mass and width of the Z^0 and $g = G_F(8\sqrt{2}\pi\alpha)^{-1} \approx 4.49 \cdot 10^{-5} \text{ GeV}^{-2}$. Q_f are the charges of the final state quarks; v_e and a_e , v_f and a_f are the electro-weak vector and axial vector coupling constants. For example, in the Weinberg-Salam model, one has $v_e = -1 + 4\sin^2 \theta_W$, $a_e = -1$ for leptons, $v_f = 1 - \frac{8}{3}\sin^2 \theta_W$, $a_f = 1$ for up-type quarks ($Q_f = \frac{2}{3}$), and $v_f = -1 + \frac{4}{3}\sin^2 \theta_W$, $a_f = -1$ for down-type quarks ($Q_f = -\frac{1}{3}$). In this paper we use Standard Model couplings with $\sin^2 \theta_W = 0.226$.

The hadron tensor components H^i can be obtained from the relevant tree-level Feynman diagrams by the above projection $H^i = (-g^{\mu\nu} + q^\mu q^\nu / q^2)H_{\mu\nu}^i$. They are given by

$$H^1(y, z) = N \left[4\xi - (4 - \xi)\xi \left(\frac{1}{y^2} + \frac{1}{z^2} \right) - 4(4 - \xi) \left(\frac{1}{y} + \frac{1}{z} \right) \right]$$

$$+2(4 - \xi)(2 - \xi)\frac{1}{yz} + 2(4 + \xi)\left(\frac{y}{z} + \frac{z}{y}\right), \quad (3)$$

$$H^2(y, z) = N\xi \left[-4 - 3\xi \left(\frac{1}{y^2} + \frac{1}{z^2} \right) - 12 \left(\frac{1}{y} + \frac{1}{z} \right) + 6(2 - \xi)\frac{1}{yz} - 2 \left(\frac{y}{z} + \frac{z}{y} \right) \right] \quad (4)$$

where $N = 4\pi\alpha_s N_C C_F$. The hadron tensor component $H^2(y, z)$ features the typical chirality factor ξ which guarantees that $H^{VV} = H^{AA}$ in the limit $v \rightarrow 1$ or $m_q \rightarrow 0$.

In order to obtain the energy spectrum of the quark we integrate over the fractional energy loss variable z of the antiquark. The integration limits are given by

$$z_{\pm} = \frac{y}{4y + \xi} \left(2 - 2y - \xi \pm 2\sqrt{(1 - y)^2 - \xi} \right). \quad (5)$$

The integration is straightforward and results in the hadron tensor components

$$H^1(y) = 2N \left[\left\{ \frac{(4 - \xi)(2 - \xi)}{y} - 2(4 - \xi) + (4 + \xi)y \right\} \ln \left(\frac{z_+(y)}{z_-(y)} \right) - 2\sqrt{(1 - y)^2 - \xi} \left\{ 2\frac{4 - \xi}{y} + \frac{(4 - 3\xi)y}{4y + \xi} - \frac{(16 - \xi^2)y}{(4y + \xi)^2} \right\} \right], \quad (6)$$

$$H^2(y) = 2N\xi \left[\left\{ 3\frac{2 - \xi}{y} - 6 - y \right\} \ln \left(\frac{z_+(y)}{z_-(y)} \right) - 2\sqrt{(1 - y)^2 - \xi} \left\{ \frac{6}{y} + \frac{3y}{4y + \xi} + \frac{(4 - \xi)y}{(4y + \xi)^2} \right\} \right]. \quad (7)$$

In Fig. 1a we show the resulting y -spectra for bottom and top pair production at $\sqrt{q^2} = 500 \text{ GeV}$ using $m_b = 4.83 \text{ GeV}$, $m_t = 175 \text{ GeV}$ and a running α_s with $\alpha_s(m_Z^2) = 0.1175$ ($n_f = 5$ below $t\bar{t}$ -threshold and $n_f = 6$ above $t\bar{t}$ -threshold). Both spectra are strongly peaked towards low y -values due to the infrared (IR) singularity at $y = 0$. The differential rate for bottom pair production is much higher than that of top pair production because the phase space is much larger for bottom pair production.

Next we determine the mean energy of the quark. Up to $O(\alpha_s)$ the mean energy of the quark is defined by

$$\langle E_q \rangle = \frac{\frac{1}{2}\sqrt{q^2}\sigma(\text{Born}) + \int E_q \frac{d\sigma(\text{tree})}{dy dz} dy dz + \frac{1}{2}\sqrt{q^2}\sigma(\text{loop})}{\sigma(\text{Born}) + \sigma(\alpha_s)}, \quad (8)$$

where $\sigma(\alpha_s)$ is the $O(\alpha_s)$ cross section $\sigma(\alpha_s) = \sigma(\text{tree}) + \sigma(\text{loop})$. Note that we define our mean energy relative to the full $O(\alpha_s)$ cross section and not to the Born term cross section as done in [5]. We shall come back to this point later on. In order to make the paper self-contained we list the Born term and $O(\alpha_s)$ cross sections appearing in the denominator of

Eq. (8) in Appendix A. We have checked that the infrared (IR) singularity resulting from the tree-graph integration in the numerator of Eq. (8) cancels against the IR-singularity of the loop contribution, i.e., including the loop contribution, the mean energy of the quark is a manifestly IR-safe measure. In fact Eq. (8) can be rewritten into a more compact form by using the fractional energy loss variable y with $E_q = \frac{1}{2}\sqrt{q^2}(1-y)$. One has

$$\langle y \rangle = \langle 1 - 2E_q/\sqrt{q^2} \rangle = \frac{\int y \frac{d\sigma(\text{tree})}{dy dz} dy dz}{\sigma(\text{Born}) + \sigma(\alpha_s)}. \quad (9)$$

The calculation of the mean $\langle y \rangle$ is simpler since one only needs to compute the tree-graph contribution. This is plausible since by taking the first moment of the differential tree-graph cross section with regard to y the IR-singular piece in the tree-graph cross section is cancelled. In the following we shall refer to the mean of variables that vanish at the IR-point as tree-graph IR-safe measures. For tree-graph IR-safe measures such as $\langle y \rangle$ the perturbation series starts at $O(\alpha_s)$. At this order the inclusion of the full $O(\alpha_s)$ total cross section in the denominator of Eq. (9) is no longer mandatory. By keeping the full $O(\alpha_s)$ contribution in the denominator one partially includes higher order effects in the evaluation of $\langle y \rangle$. In order to be definite, we shall always present our results on tree-graph IR-safe measures normalized to the full $O(\alpha_s)$ cross section.

We give the results of the first moment integration of the numerator of Eq. (9) in terms of the first moments $H^{i[y]}$ of the two relevant hadron tensor components defined by

$$H^{i[y]} = \int y H^i(y, z) dy dz. \quad (10)$$

We obtain

$$H^{1[y]} = N \left[\frac{1}{24} (256 - 224\xi + 120\xi^2 - 8\xi^3 - 5\xi^4) t_3 - \frac{1}{36} (704 + 336\xi + 34\xi^2 + 15\xi^3) v \right] \quad (11)$$

and

$$H^{2[y]} = N\xi \left[\frac{1}{24} (128 - 120\xi + 36\xi^2 + 5\xi^3) t_3 - \frac{1}{36} (280 - 118\xi - 15\xi^2) v \right]. \quad (12)$$

Our results for the y -moments are simply related to the fractional gluon energy x -moments $H^{VV[x]} = H^{1[x]} + H^{2[x]}$ and $H^{AA[x]} = H^{1[x]} - H^{2[x]}$ calculated in [5] ($x = 2p_3q/q^2 = 2E_g/\sqrt{q^2}$) as can be seen by the following reasoning. Due to CP -invariance of the underlying interaction, the y -moments $H^{i[y]}$ for the quarks and the z -moments $H^{i[z]}$ for the antiquarks are identical, i.e. $H^{i[y]} = H^{i[z]}$. From the kinematical relation $x = y + z$ one then obtains

$$H^{i[y]} = \frac{1}{2} H^{i[x]} \quad (13)$$

as already noted in [5]. Our moment results agree with the results given in [5].

In Fig. 2a we plot the mean value of the fractional energy loss variable $\langle y \rangle = \langle 1 - 2E_q/\sqrt{q^2} \rangle$ for bottom and top pair production as a function of $\sqrt{q^2}$. We first discuss the

bottom pair production case in Fig. 2a where the mean value $\langle y \rangle$ shows a sharp rise from threshold and then levels off at higher energies. To understand the high energy behaviour we consider the limiting behaviour of the y -moments $H^{i[y]}$ as $v \rightarrow 1$. In the high energy limit $v \rightarrow 1$ or, equivalently, in the limit $m_q \rightarrow 0$ we obtain

$$H^{1[y]} \rightarrow \frac{N}{3} \left[32 \ln \left(\frac{4}{\xi} \right) - \frac{176}{3} \right], \quad H^{2[y]} \rightarrow 0. \quad (14)$$

One notes that $H^{1[y]}$ becomes mass singular in this limit due to the presence of the quark/antiquark-gluon collinear singularity. There is no inconsistency in this singular behaviour from the physics point of view because the measure $\langle y \rangle$ is no longer defined in this limit. The reason is that the energy of the quark cannot be separately measured in the collinear mass zero case. In the corresponding collinear massive configuration the energy of the quark can in fact be separately determined by e.g. a time-of-flight separation. In order to define a physically meaningful $\langle y \rangle$ in the $m_q \rightarrow 0$ limit one has to introduce an angular cut-off. For very small values of the angular cut-off one would have to exponentiate the resulting large logarithmic factor taking into account multiple gluon emission. Returning to Eq. (14) the vanishing of $H^{2[y]}$ is expected since $H^{VV} \rightarrow H^{AA}$ for $v \rightarrow 1$ or $m_q \rightarrow 0$ as mentioned before. The limiting behaviour of $\langle y \rangle$ following from Eq. (14) can be seen to be given by

$$\langle y \rangle \rightarrow \frac{\alpha_s}{\pi} \frac{32 \ln(4/\xi) - 176/3}{36(1 + \alpha_s/\pi)}. \quad (15)$$

The logarithmic growth in Eq. (15) resulting from the mass singularity is off-set by the logarithmic fall-off of α_s . Looking at Fig. 2a the mean value $\langle y \rangle$ is still slightly rising at $\sqrt{q^2} = 1000 \text{ GeV}$ showing that the approach of $\langle y \rangle$ to its asymptotic value is not very fast.

Turning to the top pair production case in Fig. 2a we first determine the threshold behaviour of $\langle y \rangle$. In the nonrelativistic limit $v \rightarrow 0$ we obtain

$$H^{1[y]} \rightarrow \frac{32}{5} N v^5 + O(v^7), \quad H^{2[y]} \rightarrow \frac{32}{5} N v^5 + O(v^7). \quad (16)$$

The limiting behaviour of the $H^{i[y]}$ can be understood in the following way. At threshold the cross section factorizes into the Born term cross section $e^+e^- \rightarrow q\bar{q}$ and a gluon production piece. For the Born term cross section the s -wave vector current contribution dominates over the p -wave axial vector current contribution leading to $H^{1[y]} \simeq H^{2[y]}$ close to threshold. The leading v^5 -behaviour of the s -wave vector current contribution has its origin in the following factors: there is one power of v from the flux factor and four powers of v from integrating the y -weight over gluon phase space. We do not dwell on the nonleading $O(v^7)$ -contributions in Eq. (16) but mention that there is some interesting physics concealed in the nonleading $O(v^7)$ -contributions as discussed in [5]. Finally, when calculating $\langle y \rangle$ one divides by the Born term cross section resulting in an overall v^4 -threshold behaviour. From what has been said about the low and high energy behaviour of $\langle y \rangle$ it is clear that close to $t\bar{t}$ -threshold the vector current contribution is the dominant contribution whereas at high energies the vector and the axial vector currents contribute equally to $\langle y \rangle$. The same

statement is true for the other linear mean values calculated in the following sections. We want to mention that the high energy limit ($v \rightarrow 1$) and nonrelativistic ($v \rightarrow 0$) limits of $\langle y \rangle$ presented in this paper are in complete agreement with the results given in [5].

The power behaved dependence of $\langle y \rangle$ on $\sqrt{q^2}$ close to top-antitop threshold is clearly visible in Fig. 2a. Away from threshold $\langle y \rangle$ starts turning over at around 500 GeV in its slow approach to asymptotia. At 500 GeV the fractional energy loss of the top quark amounts to less than 1% while at 1000 GeV the fractional energy loss is 3.77% (see Table 1).

mean value	$\sqrt{q^2} = 500 \text{ GeV}$	$\sqrt{q^2} = 1000 \text{ GeV}$
$\langle y \rangle$	0.71%	3.77%
$\langle 1 + \cos \theta_{12} \rangle$	0.41%	1.99%
$\langle y(1 + \cos \theta_{12}) \rangle$	0.06%	0.57%
$\langle y_L \rangle$	1.06%	5.19%
$\langle \sin \theta_{12} \rangle$	2.07%	7.30%
$\langle y \sin \theta_{12} \rangle$	0.19%	1.23%
$\langle y_T \rangle$	1.88%	6.06%
$\langle x \rangle$	1.43%	7.53%
$2\langle p_T \rangle / \sqrt{q^2}$	1.18%	5.46%
$\langle \theta_{12} \rangle$	1.25^0	4.62^0
ξ	0.490	0.123
v	0.714	0.997

Table 1: Mean values of different kinematical quantities in $e^+e^- \rightarrow t\bar{t}g$ for $\sqrt{q^2} = 500 \text{ GeV}$ and 1000 GeV. We also list the values of ξ and $v = \sqrt{1 - \xi}$.

3 Opening angle distribution and the mean values $\langle 1 + \cos \theta_{12} \rangle$ and $\langle \sin \theta_{12} \rangle$

Next we determine the differential distribution in the cosine of the opening angle $\cos \theta_{12}$ and the mean deviation from the anticollinearity limit $\cos \theta_{12} = -1$. The central relation is the relation between $\cos \theta_{12}$ and the (y, z) -variables which reads

$$\cos \theta_{12} = \frac{yz + y + z - 1 + \xi}{\sqrt{(1-y)^2 - \xi} \sqrt{(1-z)^2 - \xi}}. \quad (17)$$

For later purposes we need to solve Eq. (17) in terms of the y -variable. One obtains a quadratic equation in y which can be solved to give

$$y_{\pm} = \frac{(1-z)(1 - \cos \theta_{12}) + z((2-z) \cos^2 \theta_{12} - (z + \xi))}{(1+z)^2 - \cos^2 \theta_{12}((1-z)^2 - \xi)}$$

$$\pm \frac{\cos \theta_{12} \sqrt{(1-z)^2 - \xi} \sqrt{4z^2 - \xi((1-z)^2 - \xi)(1 - \cos \theta_{12})}}{(1+z)^2 - \cos^2 \theta_{12}((1-z)^2 - \xi)}. \quad (18)$$

First we discuss the differential $\cos \theta_{12}$ -distribution. With the help of relation (17) the differential (y, z) -distribution given in Eq. (1) is transformed into

$$\frac{d\sigma}{d \cos \theta_{12} dz} = \frac{d\sigma}{dy dz} \frac{\partial y}{\partial \cos \theta_{12}} \quad (19)$$

where the partial derivative is given by

$$\frac{\partial y}{\partial \cos \theta_{12}} = \frac{((1-z)^2 - \xi)^{1/2}((1-y)^2 - \xi)^{3/2}}{(1-y)(2z + \xi) - \xi(z+1)}. \quad (20)$$

After substituting for y one can then integrate Eq. (19) with regard to z . Bearing in mind that the two solutions of the quadratic equation Eq. (18) $y_{\pm} = y_{\pm}(z, \cos \theta_{12})$ have to be substituted in the hadron tensor components $H^i(y, z)$ and the Jacobian Eq. (20) it is evident that it is a cumbersome task to do the requisite z -integration analytically. Instead the integration will be done numerically.

A closer look at phase space is of great help in disentangling the z -integration limits and in determining which of the two solutions $y_{\pm} = y_{\pm}(\cos \theta_{12}, z)$ of Eq. (18) have to be substituted for the y -variable in Eqs. (3), (4) and (20). In Fig. 3 we show a plot of the (y, z) -phase space for $m_t = 175 \text{ GeV}$ and $\sqrt{q^2} = 500 \text{ GeV}$. Apart from the phase space boundaries defined by $\cos \theta_{12} = \pm 1$ we have included the contour lines $\cos \theta_{12} = 0, \pm 0.7$. All contour lines of constant $\cos \theta_{12}$ must intersect at the points $(y_A, z_A) = (1 - \sqrt{\xi}, \sqrt{\xi}(1 - \sqrt{\xi})/(2 - \sqrt{\xi}))$ and $(y_B, z_B) = (\sqrt{\xi}(1 - \sqrt{\xi})/(2 - \sqrt{\xi}), 1 - \sqrt{\xi})$ where the antiquark and the quark resp. are at rest. The reason is that at these two points the opening angle θ_{12} is no longer defined. It is evident that the upper limit of the z -integration is always given by $z_B = 1 - \sqrt{\xi}$. The lower z -limit depends on whether $\cos \theta_{12}$ is positive or negative. For positive values of $\cos \theta_{12}$ the lower limit is given by $z_A = \sqrt{\xi}(1 - \sqrt{\xi})/(2 - \sqrt{\xi})$. For negative values of $\cos \theta_{12}$ the boundary curve $z_C = z_C(\cos \theta_{12})$ can be determined by first solving for the minima of the $z = z(\cos \theta_{12}, y)$ contours in the (z, y) -plane and then by inserting the y -loci of the minima into Eq. (17). For the position of the z -minima one finds

$$y = \frac{z(2-y)}{2z+y}. \quad (21)$$

After substituting (21) into Eq. (17) one obtains a quartic equation for $z_C = z_C(\cos \theta_{12})$. From the four solutions of the quartic equation the one relevant to the case at hand is given by

$$z_C = \frac{-\xi(1 - \cos \theta_{12}) + \sqrt{\xi(1 - \cos \theta_{12})(4(1 - \xi) + \xi^2(1 - \cos \theta_{12}))}}{4 - \xi(1 - \cos \theta_{12})}. \quad (22)$$

In Fig. 4 we show a plot of the phase space in the $(z, \cos \theta_{12})$ -plane with boundary curves as determined by the above discussion. We have also indicated which of the two solutions of

the quadratic equation $y_{\pm} = y(z, \cos \theta_{12})$ of Eq. (18) have to be used in the two respective phase space regions $1 \leq \cos \theta_{12} \leq 0$ and $0 \leq \cos \theta_{12} \leq -1$.

In Fig. 1b we finally show the differential $\cos \theta_{12}$ -distribution for bottom and top pair production again at the center of mass energy of 500 GeV. As expected the distributions are strongly peaked towards the IR-point at $\cos \theta_{12} = -1$. The differential bottom cross section dominates over the differential top cross section because of its larger phase space.

Next we determine the mean deviation from the anticollinearity limit $\cos \theta_{12} = -1$. To $O(\alpha_s)$ the mean of $\cos \theta_{12}$ is defined by

$$\langle \cos \theta_{12} \rangle = \frac{-\sigma(Born) + \int \cos \theta_{12} \frac{d\sigma(tree)}{dy dz} dy dz - \sigma(loop)}{\sigma(Born) + \sigma(\alpha_s)}. \quad (23)$$

Again we have checked by explicit calculation that the IR-singularity from the tree graph integration is cancelled by the corresponding IR-singularity of the loop contribution. Similar to Eq. (9) one may banish the IR-singularity in the tree graph contribution by taking the moment with regard to the weight factor $(1 + \cos \theta_{12})$. In explicit form one adds and subtracts unity in the tree-graph integral, $\cos \theta_{12} = 1 + \cos \theta_{12} - 1$. One can then rewrite Eq. (23) as

$$\langle 1 + \cos \theta_{12} \rangle = \frac{\int (1 + \cos \theta_{12}) \frac{d\sigma(tree)}{dy dz} dy dz}{\sigma(Born) + \sigma(\alpha_s)}. \quad (24)$$

What is needed are the first moment integrals $H^{i[t]}$ taken with regard to the moment variable $t = 1 + \cos \theta_{12}$ for the numerator functions. Since $\langle 1 + \cos \theta_{12} \rangle$ is a tree-graph IR-safe measure one needs to consider only the tree-graph components of the $O(\alpha_s)$ hadron tensor as explicated after Eq. (9). The requisite moment integrations can be done analytically. In fact similar integrations appear in the calculation of longitudinal spin-spin correlations [8, 9], and some of the analytical results can be taken from these papers. One obtains

$$\begin{aligned} H^{1[t]} = & N \left[8 + 16\sqrt{\xi} - 62\xi + 56\xi\sqrt{\xi} + 3\xi^2 + 3\xi^2\sqrt{\xi} + 4(4 - 5\xi - 5\xi^2)\frac{1}{v} \right. \\ & + (128 - 128\xi - 12\xi^2 + 39\xi^3 - 3\xi^4 - 32(4 - \xi)v^3) \frac{t_3}{4v^2} \\ & + 2(4 - \xi)(2 - \xi)(t_9 - t_{16}) - (64 - 48\xi - 116\xi^2 + 31\xi^3 - 3\xi^4) \frac{t_{13}}{2v^2} \\ & \left. - 4(4 + \xi)(1 - 2\xi)t_{14} + 2(16 - 40\xi + 31\xi^2 - 10\xi^3) \frac{t_{15}}{v^3} \right], \quad (25) \end{aligned}$$

$$\begin{aligned} H^{2[t]} = & N\xi \left[98 - 68\sqrt{\xi} - 3\xi - 3\xi\sqrt{\xi} - 4(7 - \xi)\frac{1}{v} + 3(32 - 25\xi^2 + \xi^3 - 96v^3) \frac{t_3}{4v^2} \right. \\ & + 6(2 - \xi)(t_9 - t_{16}) + (208 - 168\xi + 35\xi^2 - 3\xi^3) \frac{t_{13}}{2v^2} \\ & \left. - 4(13 + 3\xi)t_{14} + 6(4 - 13\xi + 8\xi^2) \frac{t_{15}}{v^3} \right]. \quad (26) \end{aligned}$$

The rate functions t_i (for $i = 3, 9, 13, 14, 15, 16$) appearing in Eqs. (25) and (26) are listed in Appendix B. As will be discussed in Sec. 4, $\langle 1 + \cos \theta_{12} \rangle$ together with $\langle y \rangle$ determine the leading contribution to the mean of the longitudinal energy $\langle E_L \rangle$.

In Fig. 2b we show a plot of the $\sqrt{q^2}$ -dependence of $\langle 1 + \cos \theta_{12} \rangle$ for bottom and top production. In the bottom case $\langle 1 + \cos \theta_{12} \rangle$ shows a quick rise from threshold and very quickly reaches its asymptotic value away from threshold. The asymptotic value is determined by the limiting behaviour of the t -moments in the high energy limit $v \rightarrow 1$. These are given by

$$H^{1[t]} \rightarrow 24N, \quad H^{2[t]} \rightarrow 0, \quad (27)$$

which translates into

$$\langle 1 + \cos \theta_{12} \rangle \rightarrow \frac{\alpha_s}{\pi} \frac{2}{1 + \alpha_s/\pi}. \quad (28)$$

In Fig. 2b we show a plot of the energy dependence of $\langle 1 + \cos \theta_{12} \rangle$ for bottom pair production. After a steep rise from threshold the mean value $\langle 1 + \cos \theta_{12} \rangle$ starts to decrease again at around 200 GeV. The logarithmic fall-off which sets in beyond 200 GeV is due to the combined effect of $\langle 1 + \cos \theta_{12} \rangle$ reaching its asymptotic value and the logarithmic running of the coupling constant α_s .

Turning to top pair production in Fig. 2b we first discuss the threshold behaviour of $\langle 1 + \cos \theta_{12} \rangle$. In the nonrelativistic limit $v \rightarrow 0$ the threshold dependence of the moments $H^{i[t]}$ is given by

$$H^{1[t]} \rightarrow \frac{256}{75} N v^5 + O(v^7), \quad H^{2[t]} \rightarrow \frac{256}{75} N v^5 + O(v^7). \quad (29)$$

One thus again has a v^4 -threshold behaviour for the mean $\langle 1 + \cos \theta_{12} \rangle$. The v^4 -threshold behaviour can clearly be discerned in Fig. 2b. At around 600 GeV $\langle 1 + \cos \theta_{12} \rangle$ starts turning over in its approach to its asymptotic value. Numerical values of $\langle 1 + \cos \theta_{12} \rangle$ for top pair production are given in Table 1.

Next we determine the mean value of $\sin \theta_{12}$ which, according to the discussion in Sec. 4, gives the leading contribution to the mean transverse energy of the quark. The mean value $\langle \sin \theta_{12} \rangle$ provides another measure of how much gluon radiation distorts the lowest order back-to-back configuration of the quark–antiquark pair. First we express $\sin \theta_{12}$ in terms of the (y, z) -phase space variables. One has

$$\sin \theta_{12} = \frac{\sqrt{4yz(1-y-z) - \xi(y+z)^2}}{\sqrt{(1-y)^2 - \xi} \sqrt{(1-z)^2 - \xi}}. \quad (30)$$

Similar to $\langle 1 + \cos \theta_{12} \rangle$ the mean value of $\sin \theta_{12}$ is determined in terms of the $O(\alpha_s)$ tree graph contribution alone since $\sin \theta_{12}$ vanishes at the IR-singular point. In the terminology of the previous sections $\langle \sin \theta_{12} \rangle$ is a tree-graph IR-safe measure. The necessary integrations have been done numerically. The top production results are shown in Fig. 5b where we plot $\langle \sin \theta_{12} \rangle$ as a function of the center of mass energy $\sqrt{q^2}$. A comparison with Fig. 5a shows that $\langle \sin \theta_{12} \rangle$ is smaller than $\langle 1 + \cos \theta_{12} \rangle$ over the whole range from top–antitop threshold

to 1000 GeV. Qualitatively this is not difficult to understand since close to the IR-point $\cos \theta_{12} = -1$ where the cross section is largest the weight function $\sin \theta_{12} = \sqrt{1 - \cos^2 \theta_{12}}$ clearly dominates over the weight $\cos \theta_{12}$ when considered as functions of $\cos \theta_{12}$. In fact $\sin \theta_{12}$ has an infinite slope at the IR-point compared to the unit slope of $\cos \theta_{12}$. One therefore expects $\langle 1 + \cos \theta_{12} \rangle < \langle \sin \theta_{12} \rangle$ which is quantitatively borne out as Figs. 5a and 5b show. Numerical values for $\langle \sin \theta_{12} \rangle$ at the two center of mass energies 500 and 1000 GeV are listed in Table 1.

Of interest is also the mean value of the opening angle θ_{12} or its complement, the acollinearity angle $\bar{\theta}_{12} = 180^\circ - \theta_{12}$. In Fig. 6 we show a plot of the energy dependence of the mean of the acollinearity angle $\langle \bar{\theta}_{12} \rangle$. $\langle \bar{\theta}_{12} \rangle$ rises smoothly from threshold to a value of 1.25° at 500 GeV and further to 4.62° at 1000 GeV. A good estimate of $\langle \bar{\theta}_{12} \rangle$ can be obtained by inverting the corresponding numerical values for $\langle \sin \theta_{12} \rangle$ in Table 1 which gives $\arcsin(\langle \sin \theta_{12} \rangle) = 1.19^\circ$ and 4.19° , respectively. Using instead $\langle 1 + \cos \theta_{12} \rangle$ for the corresponding estimate one obtains 5.16° and 11.45° which considerably overestimates the true values of $\langle \bar{\theta}_{12} \rangle$. The reason that $\langle \sin \theta_{12} \rangle$ gives a good estimate of the mean of the acollinearity angle $\langle \bar{\theta}_{12} \rangle$ can again be traced to the fact that the weight factor $\sin \theta_{12}$ (considered as function of $\cos \theta_{12}$) has a strong support close to the IR-point $\cos \theta_{12} = -1$.

4 Mean values of the transverse and longitudinal energy

Up to now we have been separately considering the energy loss of the quark and the deviation of the acollinearity angle θ_{12} from the anticollinearity limit $\theta_{12} = 180^\circ$ due to gluon radiation. From the physics point of view it is also interesting to consider the energy loss of the quark projected in the longitudinal direction as well as the build-up of transverse energy resulting from gluon radiation. Here the longitudinal and transverse energies are defined relative to the momentum direction of the antiquark and are thus defined by $E_L = -E_q \cos \theta_{12}$ and $E_T = E_q \sin \theta_{12}$. Again we shall calculate mean values of these two quantities as a measure of the importance of gluon radiation. As before we rewrite $\langle E_L \rangle$ and $\langle E_T \rangle$ in terms of tree-graph IR-safe measures. For the mean longitudinal energy one has

$$\langle E_L \rangle = \frac{1}{2} \sqrt{q^2} \left[1 - \langle 1 + \cos \theta_{12} \rangle - \langle y \rangle + \langle y(1 + \cos \theta_{12}) \rangle \right] \quad (31)$$

or, written in terms of the fractional longitudinal energy loss variable $y_L = 1 - 2E_L/\sqrt{q^2}$, one has

$$\langle y_L \rangle = \left[\langle 1 + \cos \theta_{12} \rangle + \langle y \rangle - \langle y(1 + \cos \theta_{12}) \rangle \right]. \quad (32)$$

The mean values appearing in Eq. (32) must satisfy three geometrical inequalities which follow from the geometrical inequalities $y \leq y_L$, $(1 + \cos \theta_{12}) \leq y_L$ and $y - y(1 + \cos \theta_{12}) \leq y_L$. Since these inequalities are true on an event-by-event basis they must also hold for their means. One can check that the relevant numerical entries in Table 1 satisfy the three

inequalities. On top of the geometrical inequalities one may classify the mean values of the different weight variables in Eq. (32) in terms of powers of smallness since the differential cross section is strongly peaked towards the IR-region. Thus one expects that the leading contributions to $\langle E_L \rangle$ come from the linear terms $\langle 1 + \cos \theta_{12} \rangle$ and $\langle y \rangle$ whereas the quadratically small term $\langle y(1 + \cos \theta_{12}) \rangle$ is expected to be a nonleading effect. This qualitative picture is borne out by the numerical values in Table 1 and by the curves in Fig. 5a where the energy dependence of the above mean values are combined in one common plot.

The mean of the fractional transverse energy $y_T = 2E_T/\sqrt{q^2}$ can be written as

$$\langle y_T \rangle = \left[\langle \sin \theta_{12} \rangle - \langle y \sin \theta_{12} \rangle \right]. \quad (33)$$

One now has the geometrical inequality $\langle y_T \rangle \leq \langle \sin \theta_{12} \rangle$ which can be seen to be satisfied by the relevant numerical entries in Table 1. The leading contribution is expected to arise from the linear term $\langle \sin \theta_{12} \rangle$ whereas the contribution of the term $\langle y \sin \theta_{12} \rangle$ is nonleading. The numerical values in Table 1 as well as the relevant curves in Fig. 5b confirm this picture.

Even though we do not present numerical results for the bottom production case we list the high energy limits of the mean values $\langle y(1 + \cos \theta_{12}) \rangle$, $\langle \sin \theta_{12} \rangle$ and $\langle y \sin \theta_{12} \rangle$ appearing in Eqs. (32) and (33) for the sake of completeness. Including also the result Eq. (28) one has

$$\begin{aligned} \langle 1 + \cos \theta_{12} \rangle &\rightarrow \frac{\alpha_s}{\pi} \frac{2}{1 + \alpha_s/\pi}, \\ \langle y(1 + \cos \theta_{12}) \rangle &\rightarrow \frac{\alpha_s}{\pi} \frac{20}{27(1 + \alpha_s/\pi)}, \\ \langle \sin \theta_{12} \rangle &\rightarrow \frac{\alpha_s}{\pi} \frac{10\pi}{9(1 + \alpha_s/\pi)}, \\ \langle y \sin \theta_{12} \rangle &\rightarrow \frac{\alpha_s}{\pi} \frac{\pi}{2(1 + \alpha_s/\pi)}. \end{aligned} \quad (34)$$

Where applicable the limiting values can be seen to satisfy the geometrical inequalities written down before. The limiting values show the same hierarchy in terms of powers of smallness as discussed before for top production below 1000 GeV. However, the hierarchy is not as pronounced as in the top production case below 1000 GeV. As concerns the limiting values in Eqs. (34) we want to add two remarks. In the mass zero limit treated above the transverse energy of the quark is equal to its transverse momentum. Also the mean of the longitudinal energy $\langle E_L \rangle$ and the longitudinal fractional energy loss $\langle y_L \rangle$ in Eqs. (31) and (32) are mass singular as manifested by the contribution of $\langle y \rangle$ to $\langle E_L \rangle$ and $\langle y_L \rangle$ which by itself is mass singular (see Sec. 2).

As Table 1 shows, gluon radiation causes an average energy loss of 1.06% of the top quark's energy in the longitudinal direction and an average energy gain of 1.88% in the transverse direction at this energy. At 1000 GeV the corresponding percentage figures are 5.19% and 6.06%. This has to be compared with the total energy loss of 0.71% at

500 GeV and 3.77% at 1000 GeV as calculated in Sec. 2. The gain in transverse energy is larger than the loss of longitudinal energy in this energy range where this effect becomes smaller as the center of mass energy increases. Qualitatively this behaviour may be understood from what is referred to as the “dead-cone” effect of gluon emission from a heavy quark [10]. Gluon emission is suppressed in an angular cone of size $\theta \simeq \sqrt{\xi} = 2m_q/\sqrt{q^2}$ around the quark–antiquark direction, i.e. the emitted gluon has a strong momentum component transverse to the quark–antiquark direction. Because of momentum conservation the transverse momentum of the gluon has to be balanced by the transverse momentum of the quark. A good estimate of the fractional transverse momentum of the heavy quark in the energy region under consideration can be obtained by rescaling y_T by the factor $v = p/E = 2p/\sqrt{q^2}$ where p is the lowest order momentum of the quark (see Table 1). Taking the rescaled values of $\langle y_T \rangle$ and comparing it to the mean fractional total energy of the gluon $\langle x \rangle$ in Table 1 one concludes from momentum conservation that, on average, the gluon must have a large transverse momentum or energy component. By comparing the relevant numbers at 500 and 1000 GeV one notes that this effect becomes smaller as the energy is raised in agreement with the shrinking of the “dead-cone” predicted in [10].

In order to get a more quantitative handle on the “dead-cone” effect we show a plot of the q^2 -dependence of the mean fractional gluon energy (or momentum) $\langle 2E_g/\sqrt{q^2} \rangle = \langle x \rangle$ and the mean fractional transverse momentum $\langle 2p_T/\sqrt{q^2} \rangle$ of the top in Fig. 7. In the whole range from threshold up to 1000 GeV the mean transverse momentum of the top quark is almost balanced by the mean total momentum of the gluon where the approximate equality of the two means degrades as the energy increases. This proves that the emitted gluon has a dominant transverse momentum component, and that the preference for transverse emission is degraded as the energy increases, just as expected from the “dead-cone” effect.

5 Summary and conclusions

We have discussed in some detail how gluon radiation affects the lowest order back-to-back configuration of pair produced top quarks in e^+e^- annihilation. We have introduced various measures that serve to quantify gluon radiation effects in this reaction and we have studied their energy dependence. These measures are related to the overall energy loss and the energy loss in the longitudinal direction, or, in the case of the transverse energy, to the energy gain in the transverse direction. We have also introduced two angular measures related to the opening angle θ_{12} between quark and antiquark.

When possible we have given analytical expressions for the energy and momentum measures $\langle E_q \rangle$, $\langle E_T \rangle$, $\langle E_L \rangle$ and $\langle p_T \rangle$ and for the angular measures $\langle 1 + \cos \theta_{12} \rangle$ and $\langle \sin \theta_{12} \rangle$. We have provided numerical results for all these measures in the energy range from close to top–antitop threshold up to 1000 GeV. For some of the measures we have compared the top–antitop results to the corresponding figures for bottom pair production including a discussion of the high energy limit $v \rightarrow 1$ limits of the various measures. The numerical predictions and their energy dependence can directly be compared to experimental data on top pair production at the proposed future linear colliders. The values of these mea-

tures also serve to quantify the effect of gluon radiation on the lowest order back-to-back configuration of the produced top quark pairs.

Compared to the lowest order energy of the top $E_q = \frac{1}{2}\sqrt{q^2}$ the mean loss of longitudinal energy is smaller than the mean gain in transverse energy in the range of c.m. energies from threshold to 1000 GeV. At 500 GeV the mean transverse energy exceeds the mean longitudinal energy loss by about a factor of two. In this sense the top quark is more rigid in the longitudinal direction than in the transverse direction. This behaviour can be traced to an effect which is referred to as the “dead-cone” effect in the literature. In massive quark pair production with additional gluon radiation the gluon tends to be emitted away from the heavy quark and antiquark directions. Since the mean momentum of the gluon is comparatively large ($\langle x \rangle = 2\langle y \rangle$) and since the transverse momentum of the gluon has to be balanced by the transverse motion of the quark (or antiquark) one obtains comparatively large values for the mean transverse energy and momentum of the quark (or antiquark).

Appendix A: $O(\alpha_s)$ cross section

The complete $O(\alpha_s)$ cross section for heavy quark production in $e^+e^- \rightarrow q\bar{q}g$ has been calculated before in [6, 7]. In order to make the paper self-contained we list the results in this Appendix. For the Born term cross section $\sigma(Born)$ one obtains

$$\sigma(Born) = (g_{11}\sigma^1(Born) + g_{12}\sigma^2(Born)) \quad (A1)$$

where

$$\sigma^1(Born) = \frac{\pi\alpha^2vN_C}{3q^2}(4 - \xi), \quad \sigma^2(Born) = \frac{\pi\alpha^2vN_C}{3q^2}3\xi. \quad (A2)$$

The $O(\alpha_s)$ tree- and loop-contributions are given in terms of the hadron tensor components H^i defined in Eq. (1). One has

$$H^1(\alpha_s) = N\left[\frac{3}{2}(4 - \xi)(2 - \xi)v + \frac{1}{4}(192 - 104\xi - 4\xi^2 + 3\xi^3)t_3 - 2(4 - \xi)(2 - \xi)(t_8 - t_9) - 4(4 - \xi)v(t_{10} + 2t_{12})\right], \quad (A3)$$

$$H^2(\alpha_s) = N\xi\left[\frac{3}{2}(18 - \xi)v + \frac{3}{4}(24 - 8\xi - \xi^2)t_3 - 6(2 - \xi)(t_8 - t_9) - 12v(t_{10} + 2t_{12})\right]. \quad (A4)$$

The rate functions t_i (for $i = 3, 8, 9, 10, 12$) are given in Appendix B.

Appendix B: Rate integrals and first moment integrals

The analytical expressions of the $O(\alpha_s)$ cross section and the mean value $\langle 1 + \cos\theta_{12} \rangle$ involve a number of basic rate functions which are collected in this Appendix.

$$t_3 = \ln\left(\frac{1+v}{1-v}\right),$$

$$\begin{aligned}
t_8 &= \ln\left(\frac{\xi}{4}\right) \ln\left(\frac{1+v}{1-v}\right) + \text{Li}_2\left(\frac{2v}{1+v}\right) - \text{Li}_2\left(-\frac{2v}{1-v}\right) - \pi^2, \\
t_9 &= 2 \ln\left(\frac{2(1-\xi)}{\sqrt{\xi}}\right) \ln\left(\frac{1+v}{1-v}\right) + 2\left(\text{Li}_2\left(\frac{1+v}{2}\right) - \text{Li}_2\left(\frac{1-v}{2}\right)\right) + \\
&\quad + 3\left(\text{Li}_2\left(-\frac{2v}{1-v}\right) - \text{Li}_2\left(\frac{2v}{1+v}\right)\right), \\
t_{10} &= \ln\left(\frac{4}{\xi}\right), \quad t_{12} = \ln\left(\frac{4(1-\xi)}{\xi}\right), \quad t_{13} = \ln\left(\frac{1+v}{2-\sqrt{\xi}}\right), \\
t_{14} &= \ln\left(\frac{4}{\xi}\right) \ln\left(\frac{1+v}{2-\sqrt{\xi}}\right) \\
&\quad + 2\text{Li}_2\left(\frac{2-\sqrt{\xi}}{2}\right) - 2\text{Li}_2\left(\frac{\sqrt{\xi}}{2}\right) + \text{Li}_2\left(\frac{1-v}{2}\right) - \text{Li}_2\left(\frac{1+v}{2}\right), \\
t_{15} &= \left(\ln\left(\frac{1+v}{1-v}\right) + \ln\left(\frac{\sqrt{\xi}}{2-\sqrt{\xi}}\right)\right)^2 \\
&\quad - 4\text{Li}_2\left(\sqrt{\frac{1-v}{1+v}}\right) + 2\text{Li}_2\left(\frac{2-\sqrt{\xi}}{1+v}\right) + 2\text{Li}_2\left(\frac{1-v}{2-\sqrt{\xi}}\right), \\
t_{16} &= \ln\left(\frac{1+v}{1-v}\right) \ln\left(\frac{4v^4}{\xi(1+v)^2}\right) - \text{Li}_2\left(\frac{2v}{(1+v)^2}\right) + \text{Li}_2\left(\frac{-2v}{(1-v)^2}\right) \\
&\quad + \frac{1}{2}\text{Li}_2\left(-\frac{(1-v)^2}{(1+v)^2}\right) - \frac{1}{2}\text{Li}_2\left(-\frac{(1+v)^2}{(1-v)^2}\right). \tag{B1}
\end{aligned}$$

Appendix C: Scalar and pseudoscalar currents

In this Appendix we present expressions for the hadron tensor components and their first moments which allows one to calculate the mean values $\langle y \rangle$ and $\langle 1 + \cos\theta_{12} \rangle$ for the scalar (S) and pseudoscalar (P) current contributions $H^1 = \frac{1}{2}(H^{SS} + H^{PP})$ and $H^2 = \frac{1}{2}(H^{SS} - H^{PP})$. These expressions would be needed for the assessment of gluon emission effects in the heavy quark production process $e^+e^- \rightarrow q\bar{q}(g)$ mediated by scalar (S) or pseudoscalar (P) particles as resulting from e.g. Higgs exchange. One has

$$H^{1[y]} = N\xi\left[\frac{3}{2}(2-\xi)v - \frac{1}{4}(8-8\xi+3\xi^2)t_3\right], \tag{C1}$$

$$H^{2[y]} = N\left[\frac{1}{6}(2-\xi)(16-16\xi+7\xi^2)t_3 - \frac{1}{9}(76-76\xi+21\xi^2)v\right], \tag{C2}$$

$$\begin{aligned}
H^{1[t]} &= N\xi\left[\frac{8\xi}{v} - 8(2-\sqrt{\xi}) - 2(4-\xi-2\xi^2-4v^3)\frac{t_3}{v^2} - 2(2-\xi)(t_9-t_{16})\right. \\
&\quad \left. - 4(4-\xi)\frac{t_{13}}{v^2} + 2(6+\xi)t_{14} - 2(4-12\xi+7\xi^2)\frac{t_{15}}{v^3}\right], \tag{C3}
\end{aligned}$$

$$H^{2[t]} = N\left[8(7-9\xi+\xi^2)\frac{1}{v} - 2(34-36\sqrt{\xi}+5\xi-7\xi\sqrt{\xi})\right]$$

$$\begin{aligned}
& +(32 - 48\xi + 15\xi^2 + 5\xi^3 - 16(2 - \xi)v^3)\frac{t_3}{2v^2} \\
& +2(2 - \xi)^2(t_9 - t_{16}) - (80 - 120\xi + 31\xi^2 - 3\xi^3)\frac{t_{13}}{v^2} \\
& +2(4 + 10\xi + \xi^2)t_{14} + 2(8 - 22\xi + 20\xi^2 - 7\xi^3)\frac{t_{15}}{v^3}].
\end{aligned} \tag{C4}$$

References

- [1] S. Parke and Y. Shadmi, *Phys. Lett.* **387 B** (1996) 199
- [2] *Proc. Workshop on Physics and Experiments at 500 GeV: The Physics Potential*, Munich–Annecy–Hamburg 1991, ed. P.M. Zerwas, DESY 92-123A,B
- [3] *Proc. Workshop on Physics and Experiments with e^+e^- linear colliders*, Saariselkä 1991, eds. R. Orava, P. Eerola and M. Nordberg, World Scientific, Singapore 1992
- [4] Y. Akatsu and O. Terazawa, *Int. J. Mod. Phys.* **A7** (1992) 1467
- [5] Yu.L. Dokshitzer, V.A. Khoze and W.J. Stirling, *Nucl. Phys.* **B428** (1994) 3
- [6] S. Groote, J.G. Körner and M.M. Tung, *Z. Phys.* **C74** (1997) 615
- [7] J.G. Körner, A. Pilaftsis and M.M. Tung, *Z. Phys.* **C63** (1994) 575
- [8] S. Groote, J.G. Körner and J.A. Leyva, Mainz preprint MZ-TH/97-27, hep-ph/9708367, to be published in *Phys. Lett. B*
- [9] J. Bernabéu, J. Peñarrocha and M.M. Tung, Valencia preprint FTUV-97/39, hep-ph/9706444, to be published in *Phys. Lett. B*
- [10] Yu.L. Dokshitzer, V.A. Khoze and S.I. Troyan, *Proc. 6th Int. Conf. on Physics in Collision*, ed. M. Derrick, World Scientific (1987), p. 417. A more accessible reference is the following text book: R.K. Ellis, W.J. Stirling and B.R. Webber, “QCD and Collider Physics”, Cambridge University Press (1996), Cambridge

Figure Captions

- Fig. 1: Differential (a) y - and (b) $\cos \theta_{12}$ -distribution for $e^+e^- \rightarrow b\bar{b}g$ and $e^+e^- \rightarrow t\bar{t}g$ at $\sqrt{q^2} = 500 \text{ GeV}$ ($m_t = 175 \text{ GeV}$, $m_b = 4.83 \text{ GeV}$)
- Fig. 2: Mean values of (a) the fractional energy loss variable y of the bottom and top quark and (b) the variable $t = 1 + \cos \theta_{12}$ as functions of $\sqrt{q^2}$ for bottom and top quark pair production ($m_t = 175 \text{ GeV}$, $m_b = 4.83 \text{ GeV}$)
- Fig. 3: (y, z) -phase space for $e^+e^- \rightarrow t\bar{t}g$ ($m_t = 175 \text{ GeV}$, $\sqrt{q^2} = 500 \text{ GeV}$). Also shown are contour lines for constant values of $\cos \theta_{12}$. To the right and to the left of the zero contour line $\cos \theta_{12} = 0$ are the phase space regions $0 \leq \cos \theta_{12} \leq 1$ and $-1 \leq \cos \theta_{12} \leq 0$. All contour lines of constant $\cos \theta_{12}$ intersect at points A and B . Point C denotes the minimum of the $\cos \theta_{12}$ contour lines for negative values of $\cos \theta_{12}$. The IR-point is at the origin.
- Fig. 4: $(z, \cos \theta_{12})$ -phase space for $e^+e^- \rightarrow t\bar{t}g$ ($m_t = 175 \text{ GeV}$, $\sqrt{q^2} = 500 \text{ GeV}$). The IR-point is at the lower left corner. The dark-shaded y_+ - and the light-shaded y_- -regions correspond to the two solutions of the quadratic equation $y_{\pm} = y_{\pm}(z, \cos \theta_{12})$
- Fig. 5: Comparison of the mean values of (a) $y_L = 1 - 2E_L/\sqrt{q^2}$, y , $1 + \cos \theta_{12}$, and $y(1 + \cos \theta_{12})$ and (b) $y_T = 2E_T/\sqrt{q^2}$, $\sin \theta_{12}$, y , and $y \sin \theta_{12}$ for top pair production in $e^+e^- \rightarrow t\bar{t}g$ as function of $\sqrt{q^2}$
- Fig. 6: Mean value of the acollinearity angle $\bar{\theta}_{12}$ in $e^+e^- \rightarrow t\bar{t}g$ as function of $\sqrt{q^2}$
- Fig. 7: Mean values of the fractional gluon energy x and fractional transverse momentum $2p_T/\sqrt{q^2}$ of the top quark in $e^+e^- \rightarrow t\bar{t}g$ as functions of $\sqrt{q^2}$

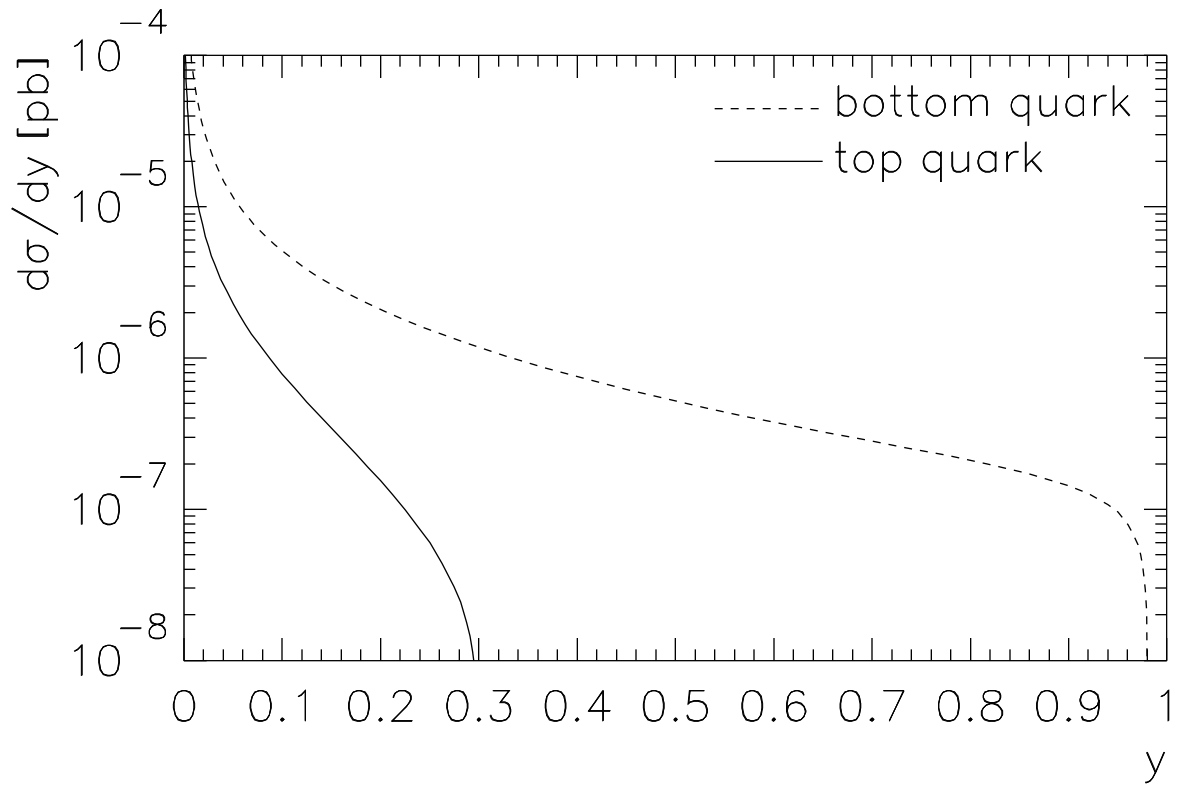


Figure 1(a)

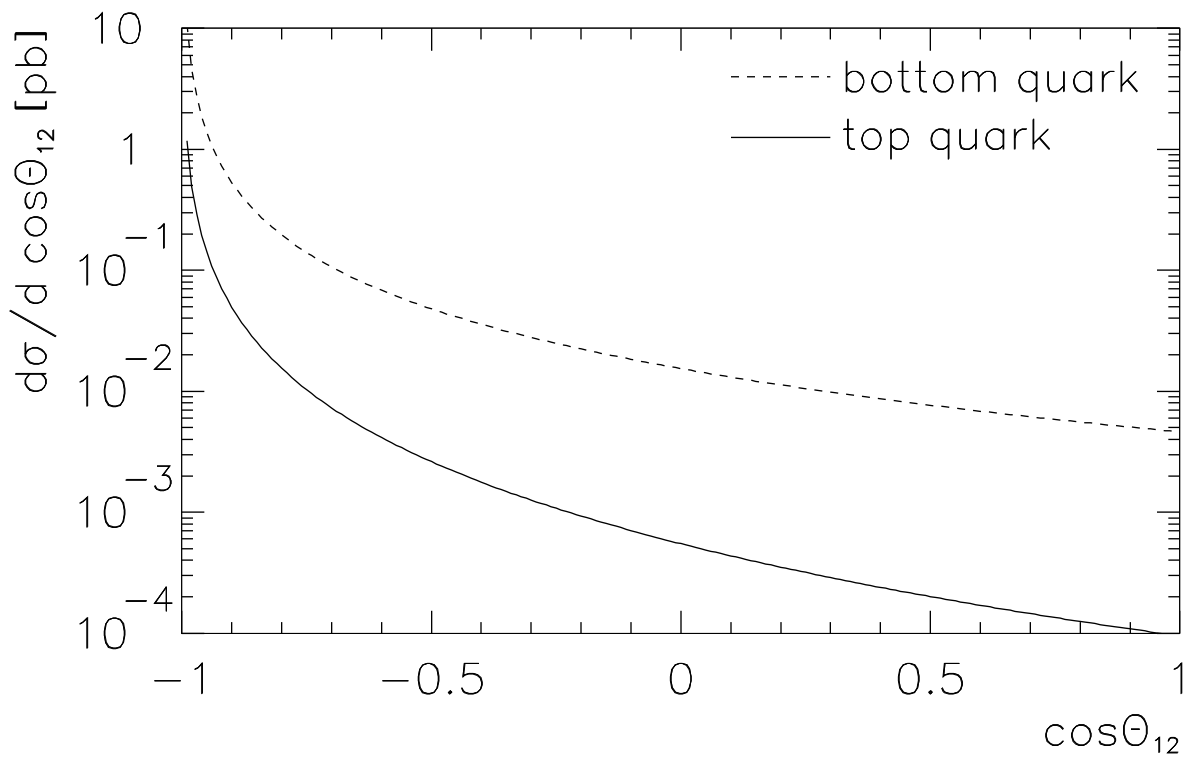


Figure 1(b)

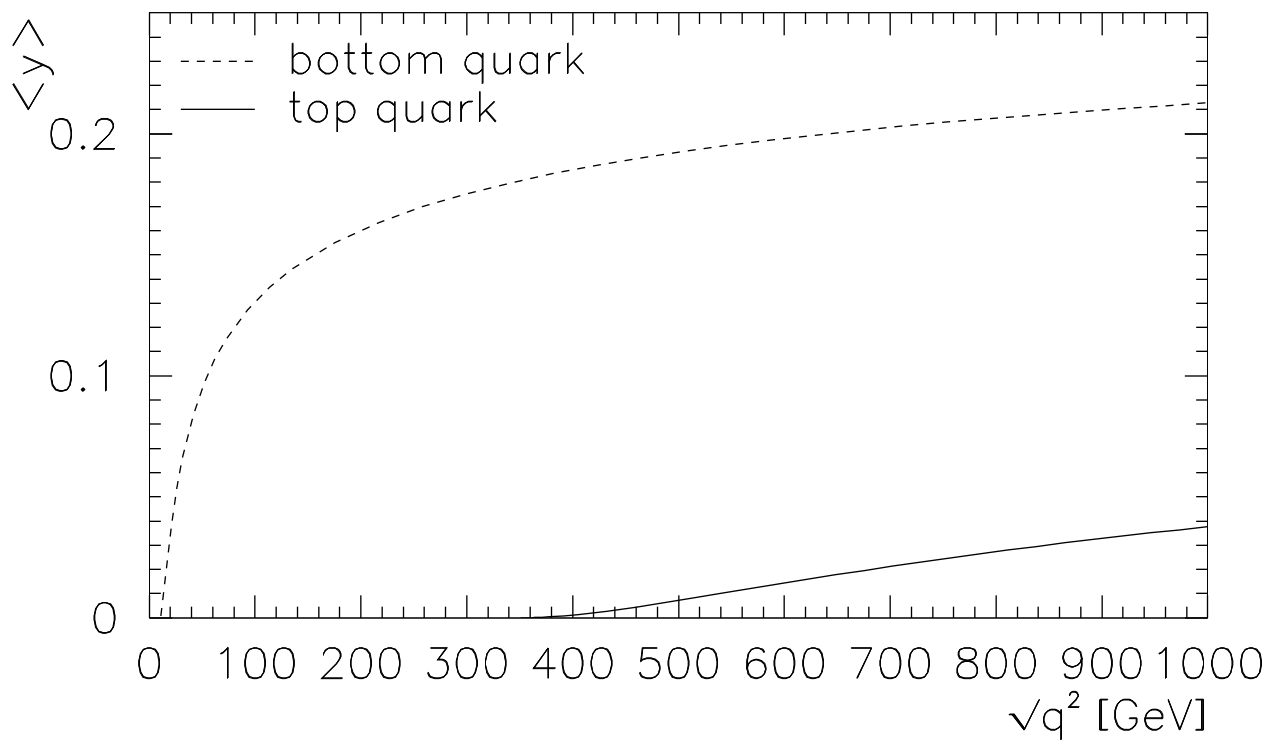


Figure 2(a)

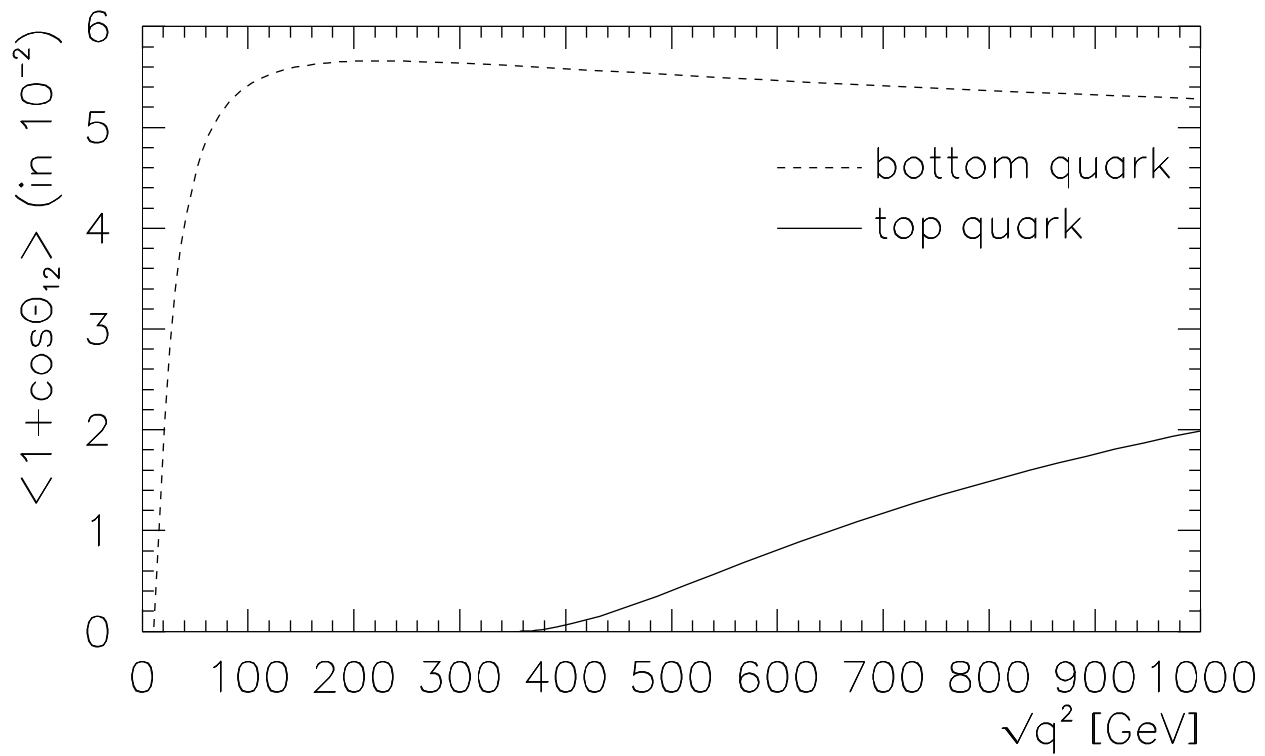


Figure 2(b)

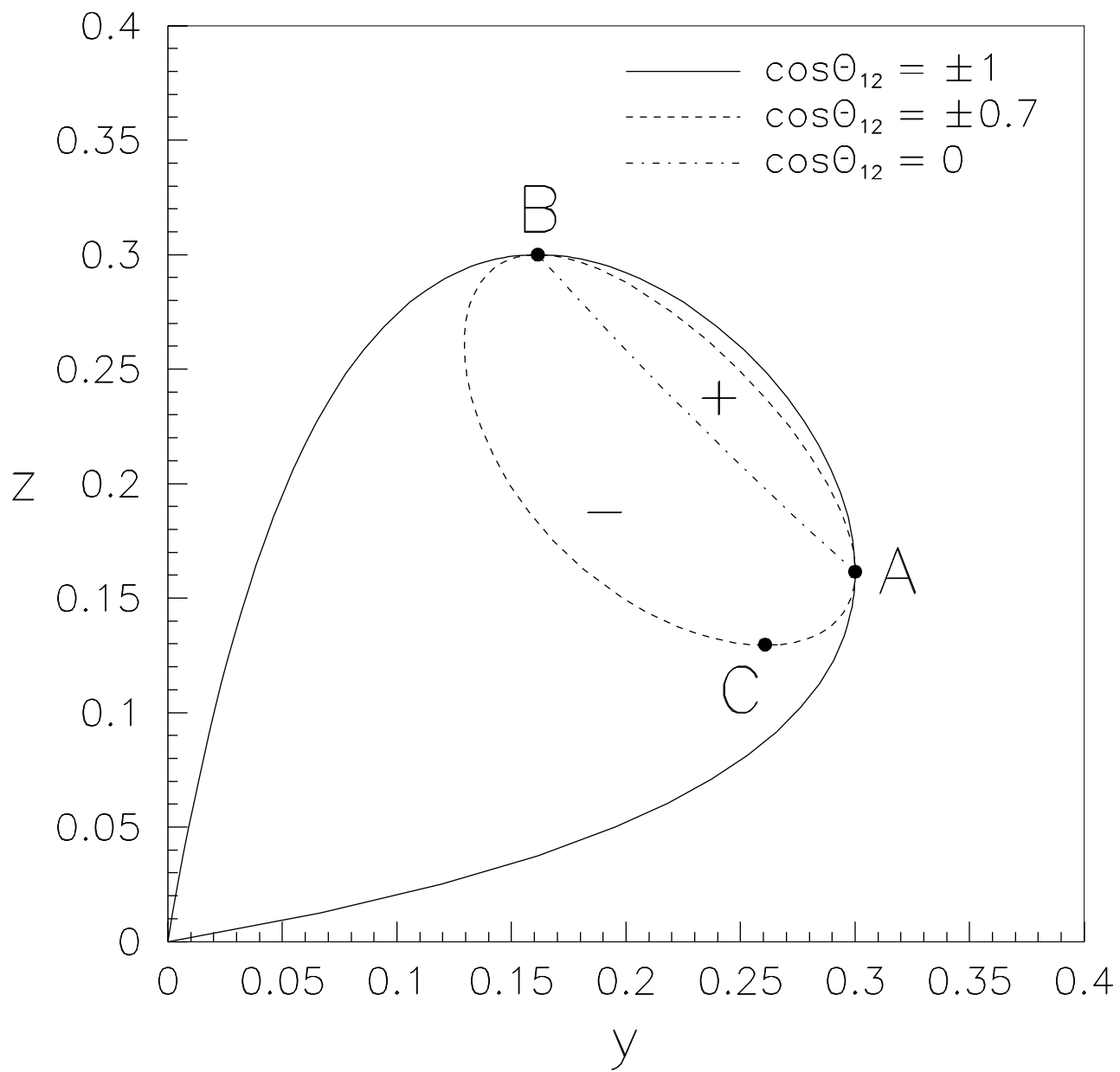


Figure 3

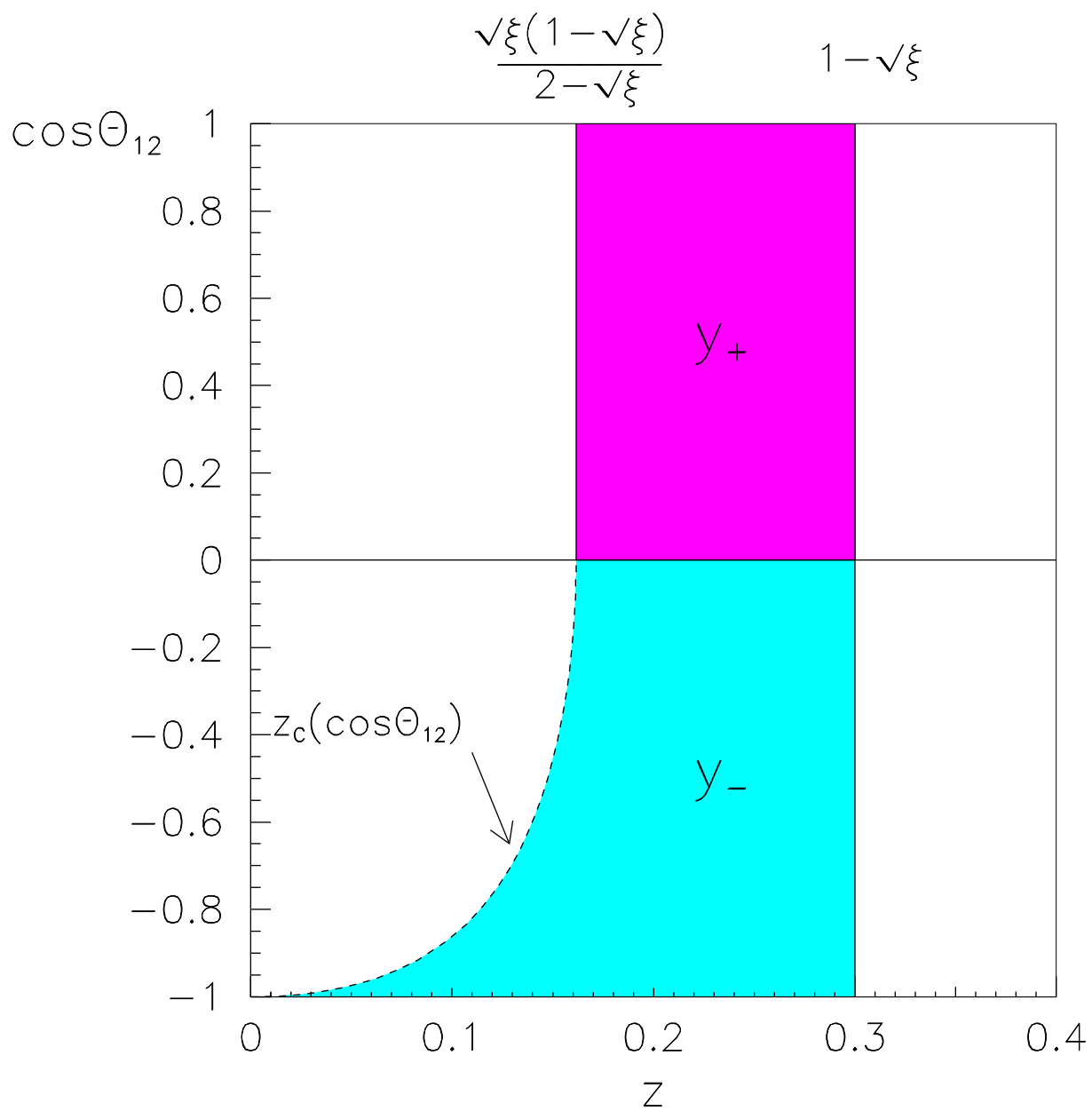


Figure 4

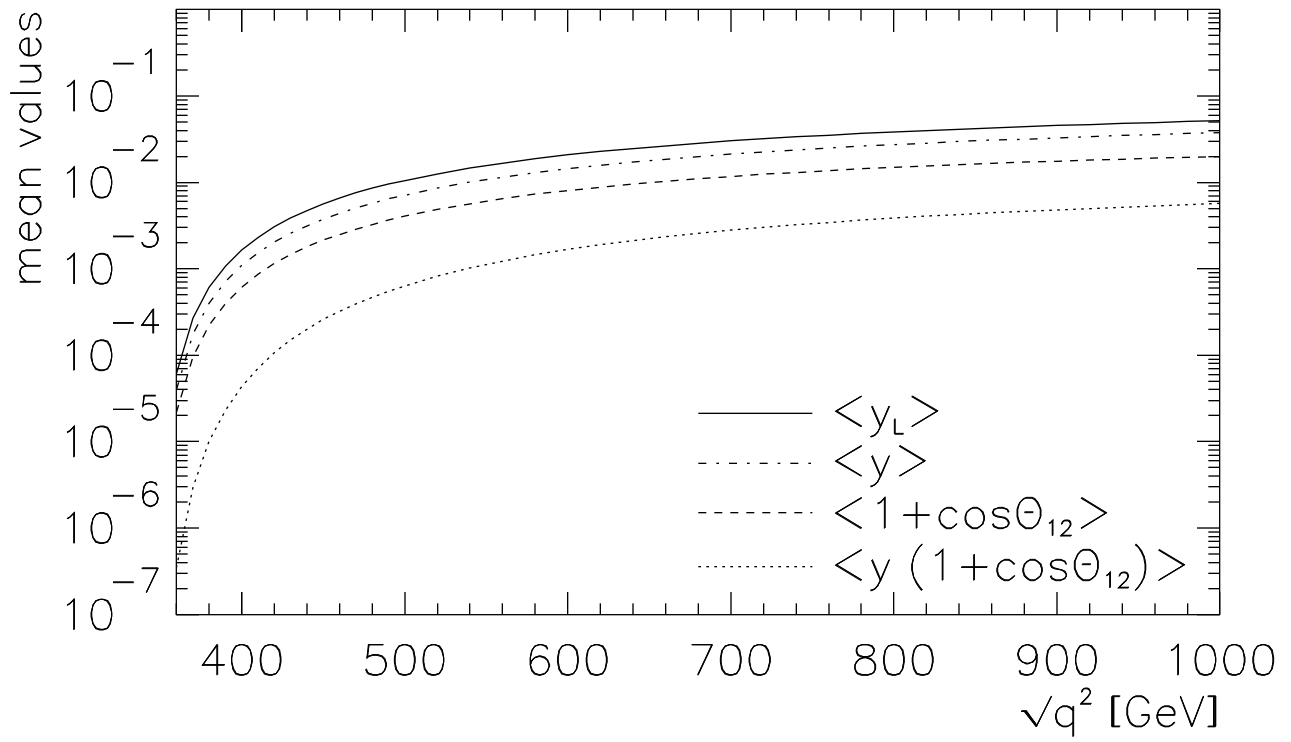


Figure 5(a)

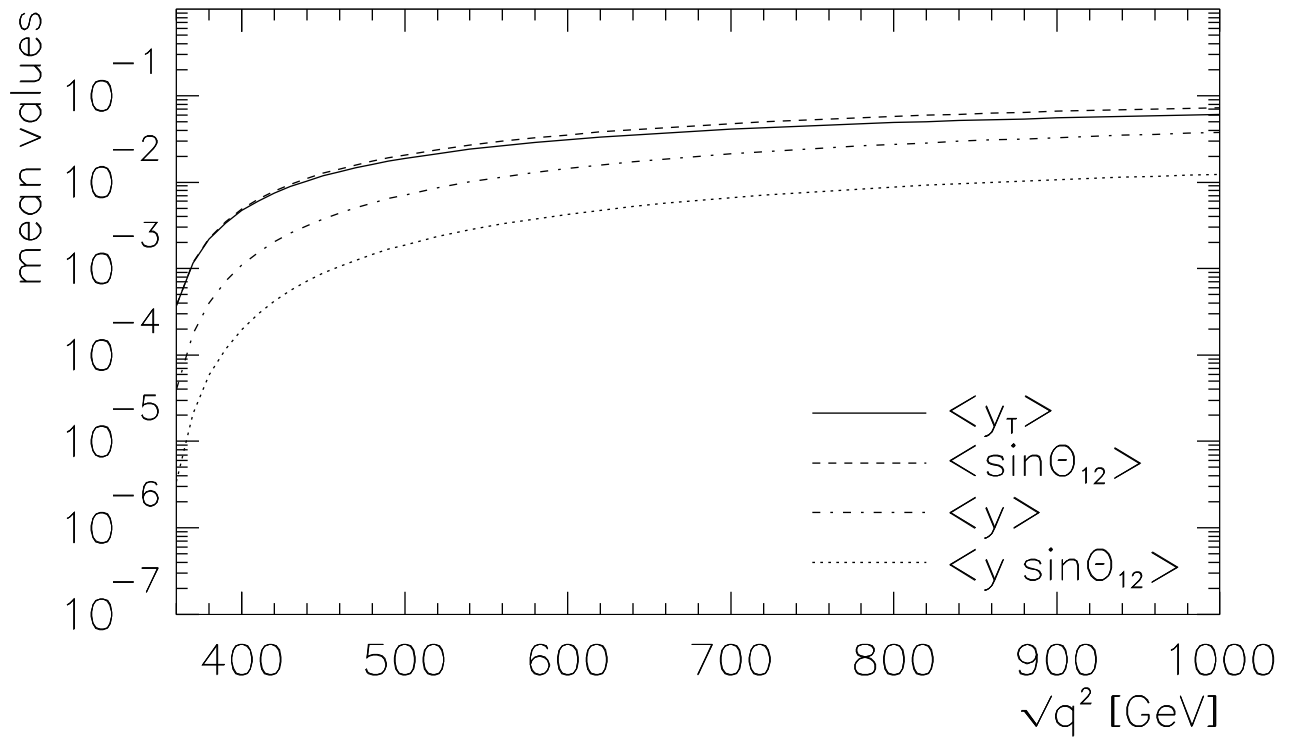


Figure 5(b)

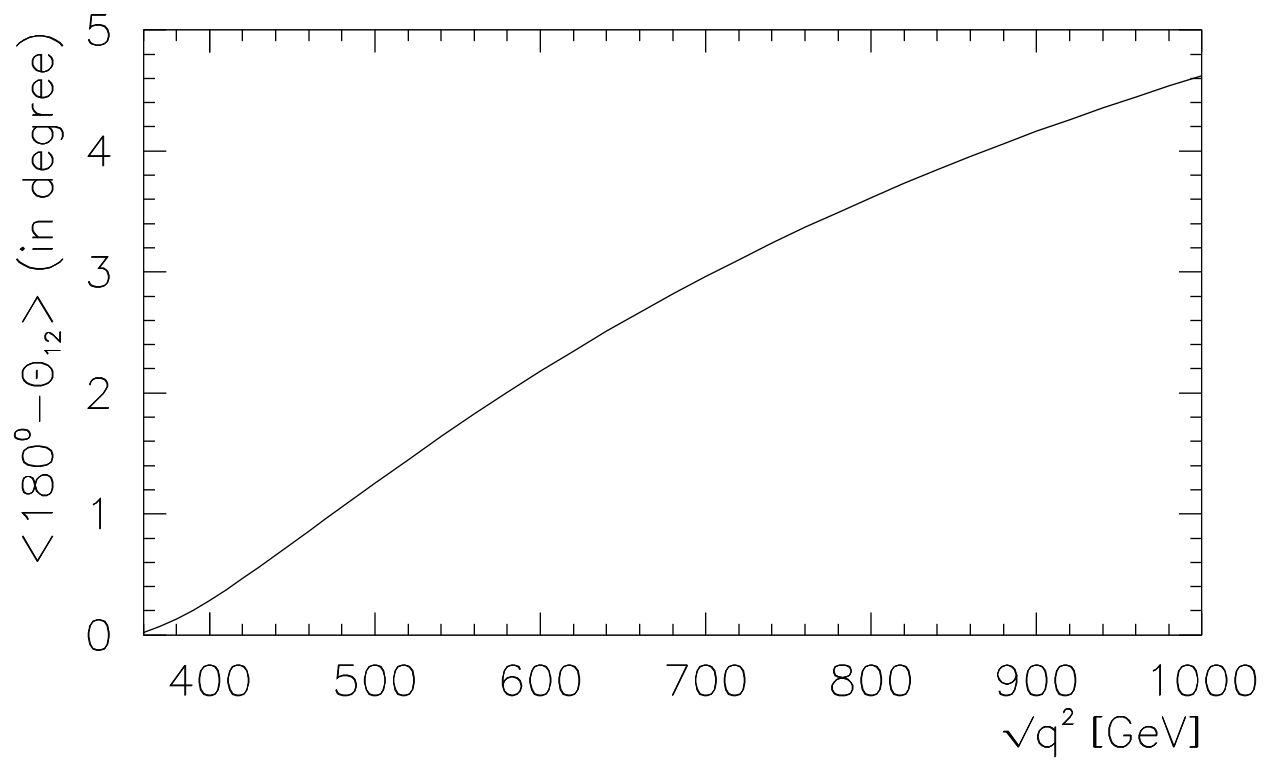


Figure 6

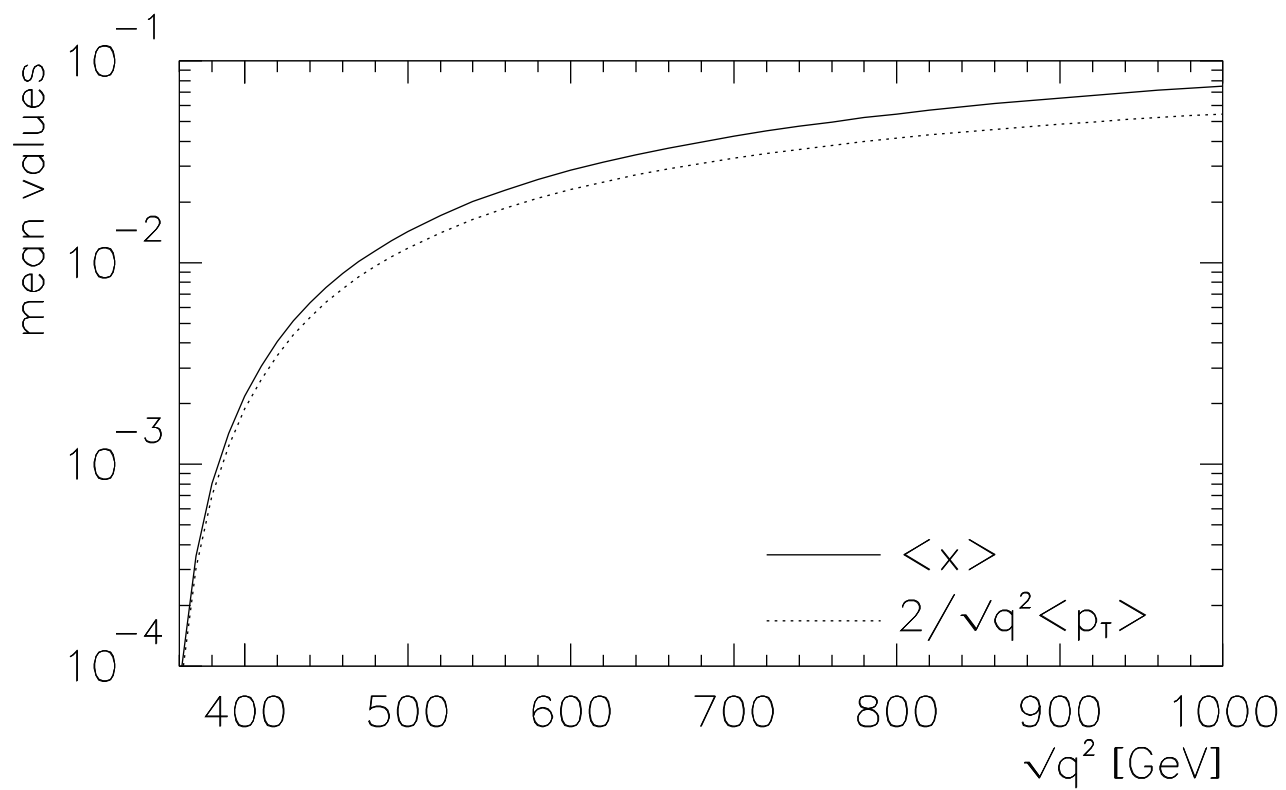


Figure 7